Chemical Engineering Science 66 (2011) 2164–2176

Contents lists available at ScienceDirect

Chemical Engineering Science

journal homepage: www.elsevier.com/locate/ces

# Crosswise ridge micromixers with split and recombination helical flows

Jyh Jian Chen [a,*], Yu Ren Lai [b], Rei Tang Tsai [c], Jenn Der Lin [d], Chih Yang Wu [c]

[a] Department of Biomechatronics Engineering, National Pingtung University of Science and Technology, 1, Hseuh Fu Road, Nei Pu, Pingtung 912, Taiwan
[b] Department of Mechanical Engineering, National Chiao Tung University, 1001, Ta Hsueh Road, Hsinchu 300, Taiwan
[c] Department of Mechanical Engineering, National Cheng Kung University, 1, University Road, Tainan 701, Taiwan
[d] Department of Power Mechanical Engineering, National Formosa University, 64, WenHua Road, Huwei Township, Yunlin 632, Taiwan

ARTICLE INFO

*Article history:*
Received 22 September 2010
Received in revised form
9 February 2011
Accepted 10 February 2011
Available online 20 February 2011

*Keywords:*
Confocal image
Passive micromixer
Slanted ridge
Mixing index
Split and recombination
Helical flows

ABSTRACT

This study presents a novel crosswise ridge micromixer (CRM) with a series of microstructures placed on the top and bottom floors of channels. Passive micromixers fabricated by Micro Electro-Mechanical Systems (MEMS) technologies with slanted ridges are investigated. Numerical simulations and experimental investigations are undertaken to determine the effects of various microstructure patterns on mixing efficiency with Reynolds numbers (*Re*) of 0.05–50. The confocal images at the cross-sections along the channel with ridges on both the channel top and bottom are first investigated in our study. A significant amount of split and recombination (SAR) helical flows is produced by the slanted ridges embedded on the two floors of the channels. The effects of non-dimensional parameters, such as the *Re*, as well as geometrical parameters on mixing performance are presented in terms of the mixing index. When the *Re* exceeds 1, the mixing index of the micromixer with slanted ridges increases as the *Re* increases further. Simulation results are presented and compared with experimental data. The trends of the experimental results and numerical data are very similar. Finally, various numbers of slanted ridges in the same orientation in one channel cycle are investigated to determine mixing performance in microchannels. The mixing performance achieves an optimum value in case where the number of ridges per cycle is equal to 8.



## 1. Introduction

Over the last decade, microfluidic technologies have earned considerable interest in a variety of disciplines. Some products have been mass-produced using an MEMS technology. Microfluidic devices have been developed for a broad range of applications in bio-analysis and chemical process technologies. Effective mixing of the fluids is essential in numerous miniaturized multi-component flow systems. Rapid mixing can reduce analysis time and improve reaction efficiency in industrial applications. In practice, both stirring and a turbulent flow are utilized to improve macroscopic mixing characteristics. The dimensions of micro-scale systems are so small that Reynolds numbers exceeding 1000 are not feasible, and only a laminar flow of liquid can be observed. Reynolds number (*Re*) is the ratio of inertia to viscous forces and is expressed as $Re=UD_H/\nu$, where $U$ is inlet flow velocity, $D_H$ is hydraulic diameter and $\nu$ is the kinematic viscosity. Notably, rapid mixing in microfluidic analytical devices cannot be achieved using conventional approaches.

In a typical microfluidic device, the mixing of two or more miscible fluid streams is achieved by molecular diffusion driven by a concentration difference; however, this process is rather slow. According to Fick's first law of diffusion, the flux of the diffusing species is proportional to the diffusivity and a gradient of the concentration (Incropera and DeWitt, 1990). Additionally, the time taken when molecules travel or diffuse increases in proportion to the square value of distance, and further depends on the diffusivity of the diffusing liquid (Cussler, 1984). To accelerate mixing, the essential mechanisms of mass transportation of a diffusion based micromixer are the maximization of the contact area of different fluids and the minimization of diffusing distance. A number of micromixers have been developed. These can be classified into two groups: active and passive micromixers. Although the time and channel length required for active mixing are less than that for passive mixing, active micromixers are difficult to fabricate, clean and integrate into microfluidic systems. The main advantage of passive micromixers is that they utilize no external power, except for that used by the mechanism delivering fluids into microfluidic systems.

For the past ten years, many studies have investigated passive mixing in micromixers. Nguyen and Wu, who reviewed existing micromixers, reported on the recent progress in the development of micromixers (Nguyen and Wu, 2005). Since generating a turbulent liquid flow on a microscale is difficult, mixing in passive

* Corresponding author. Tel.: +886 8 7723202x7029; fax: +886 8 7740420.
*E-mail address:* Chaucer@mail.npust.edu.tw (J. Jian Chen).

0009-2509/$ - see front matter © 2011 Elsevier Ltd. All rights reserved.
doi:10.1016/j.ces.2011.02.022

micromixers relies primarily on molecular diffusion and chaotic advection. By considering molecular diffusion characteristics, some researchers have examined injection mixing, where one liquid fluid is injected into the other liquid fluid with micro plumes (Miyake et al., 1993; Voldman et al., 2000). Some studies have developed micromixers based on the increase in the contact surface area via lamination (Mobius et al., 1995; Branebjerg et al., 1996). These designs separate incoming streams into several narrow confluent streams that are subsequently rejoined. The thickness of each fluid layer is markedly reduced in comparison with characteristic diffusion length, which reduces the mixing time. Although the flow-splitting technique is effective, it remains limited by diffusion. Such micromixers need sufficient space to separate fluids into several channels to allow mixing, and this may result in a marked pressure drop.

To increase the mixing rate beyond the diffusion limit, off-axis or lateral transport within the channel must be induced (Jones et al., 1989). Fortunately, mixing in such laminar flows can be enhanced through chaotic advection (Johnson et al., 2002). A chaotic mixer refers to unit operation that stretches and folds fluid volumes over a channel cross section (Ottino and Wiggins, 2004). Dynamic systems theory indicates that chaotic advection can occur when a velocity field is either two-dimensional with time-dependent perturbation or three-dimensional with or without time-dependent perturbation. Chaotic advection typically results in enhanced transverse flow, and is indicative of rapid distortion and elongation of material interfaces. This deformation significantly increases the interfacial area across which diffusion occurs, resulting in rapid mixing. Some studies achieved chaotic advection in microstructures using three-dimensional twisted channels (Liu et al., 2000), electrokinetic instability (Oddy et al., 2001), or a bas-relief structure on the channel floor (Stroock et al., 2002). The challenges of three-dimensional twisted channels are the micro-fabrication of complex structures and the need for a high *Re* to stir the fluids and generate chaotic advection. Notably a micromixer using electrokinetic instability is an active micromixer with no moving parts that can take advantage of fluctuating electrical fields to produce mixing, although, a function generator coupled with a high-voltage amplifier is needed to generate fluctuating electrical fields. Bas-relief structures, however, are conveniently useful in generating transverse flows for a wide range of *Re* without difficult fabrication or any other active parts.

Stroock et al. (2002) developed two micromixers with bas-relief structures. One is a slanted, grooved mixer (SGM) in which ridges on the channel floor form an oblique angle relative to the long axis of the channel. The other is a staggered herringbone mixer (SHM), in which a series of asymmetrical herringbone grooves are etched into the channel floor to increase mixing efficiency. The primary mixing mechanism may be splitting and reorientation due to periodic up-and-down-welling motion. Johnson et al. (2002) designed an effective SGM that has grooves slanted at 45° and/or a series of partial slanted grooves placed on the channel floor. This mixer has a high degree of lateral transport across the channel over a broad range of electro-osmotic flow rates. Some researchers numerically and/or experimentally analyzed these two micromixers to characterize mixing. Both qualitative and quantitative techniques were applied to describe the flow fields and mixing mechanisms in channels. The effects of various geometric parameters of micromixers on the mixing characteristics were also investigated (Aubin et al., 2003; Lim et al., 2003; Wang et al., 2003b; Li and Chen, 2005; Aubin et al., 2005; Yang et al., 2005; Camesasca et al., 2005; Hasssell and Zimmerman, 2006; Ansari and Kim, 2007; Cortes-Quiroz et al., 2009). The effect of the diamond ridge offsets from the channel centerline was investigated (Bhagat et al., 2007), and analytical results show that the design incorporates break-up ridges within the microchannel that achieve excellent mixing performance over a wide range of flow conditions.

To improve the mixing performance, researchers have developed micromixers with patterned grooves or ridges on both the top and bottom floors of a channel. Some have dealt with the flow characteristics of liquid in channels with grooves on two opposite walls. Schonfeld and Hardt (2004) numerically analyzed helical flows in a bas-relief-structured SGM. They showed that bas-relief grooves on two opposite walls significantly increase the relative transverse velocity compared to that in channels with structures on only one wall. Howell Jr. et al. (2005) developed a microfluidic mixer containing chevron and stripe grooves on both the channel top and bottom. This design created vertically stacked vortices, as well as two vortices adjacently positioned. In comparison with the SHM, mixing in this system is superior. The mixing fluids in microchannels, in which barriers are positioned on the channel top surface and grooves are placed on the bottom, were studied. Kim et al. (2004) examined barrier embedded micromixers (BEM) in which barriers are periodically inserted along the channel top surface and slanted grooves are placed on the channel bottom surface. They determined that the flow field in a BEM has one hyperbolic point in the velocity field of co-rotating cross-sectional flows, which inherently causes tremendous stretching around the channel. Kang and Kwon (2004) applied the colored-particle tracking method to three patterned-groove micromixers—the SGM, SHM and BEM. Their numerical results demonstrate that no notable chaotic mechanism exists in the SGM as opposed to that in the other two micromixers. Kang et al. (2008) investigated mixing characteristics of the BEM influenced by periodic and aperiodic sequences of mixing protocols for varying *Re*. The higher the *Re*, the faster and the more uniform mixing. The mixing of liquid flows was demonstrated and the ridges were fabricated onto the top and bottom floors of a channel. Fu et al. (2006) presented the staggered oriented ridges static micromixers (SOR). In every mixing segment, the microstructure consisted of microchannels and two pairs of ridges. The 45° angle characterizing the orientation of the ridges with respect to the channel is the most appropriate. Their results show that the interface between the two streams is distorted as it moves downstream, and a significant amount of stirring accompanies at a *Re* of 57.93.

In all of the aforementioned studies, two representative patterned-groove micromixers, the SGM and SHM, were analyzed comprehensively. Periodically, the barriers or slanted grooves are placed on the top surface of a microchannel with microstructures on the bottom floor in micromixers. As the strength of the helical flow increases, mixing increases (Kim et al., 2004). Bas-relief structures on two opposite walls can significantly increase mixing performance. Nevertheless, few studies numerically and experimentally investigated the influence of various geometric parameters on mixing performance of a mixer with grooves or ridges on two opposing floors. In all of the aforementioned studies, only one study considered the mixing inside the channels with ridges constructed onto the top and bottom floors. The top views of the images from CCD camera and the computational results from CFD package were used to analyze the flow. The confocal images at the cross-sections along the channel with the ridges on two floors were not investigated before. However, to verify the simulation results and monitor the mixing behaviors at the cross-sections of the mixing channel, the confocal images would be useful for analyzing the data and understanding the performance of the device. Therefore, understanding the fluid flows in crosswise ridge micromixer is of marked importance in the related fields of microfluidics.

In our crosswise ridge micromixer, there exists a distinct, strong and complex three-dimensional flow field inside the channel. We attempted to systematically analyze some numerical computations and flow visualizations, and examined the physical insights of the flow characteristics and the mixing performances in our design. This study presents a novel micromixer, in which a

series of slanted ridges are etched onto the top and bottom floors of a channel. This micromixer is fabricated using the MEMS technology. A steady state three-dimensional fluid field is utilized to describe flow characteristics in the proposed micro system. From previous studies (Aubin et al., 2003; Hasssell and Zimmerman, 2006; Ansari and Kim, 2007; Kang et al., 2008), the governing equations at steady state were utilized by the researchers concerned with the mechanisms of chaotic mixing. Their micromixers made use of a specific three-dimensional structure to induce a lateral motion of fluids in a periodic manner, giving rise to chaotic mixing. Through splitting, rotation and recombination of the fluids, global chaotic mixing can be achieved. Flow experiments are performed and compared with numerical simulation results. The effects of non-dimensional parameters for inlet velocity on flow characteristics are examined. Finally, the effects of the number of crosswise patterns with the same orientation for a cycle along the downchannel on the mixing process are presented in terms of mixing characteristics.

## 2. Mathematical model and numerical methodology

This study examines the mixing characteristics of two miscible liquids entering two branches of a passive micromixer subjected to a specific inlet pumping velocity at various values of geometrical and operational parameters. Numerical simulations are conducted to assess the mixing performances of two different liquid flows inside microchannels. It is assumed that a steady state is reached in the channel; variations in concentration do not alter fluid viscosity and density, and channel walls are smooth. The effects of surface tension on the interaction between two miscible liquids on Earth are masked by the effects of gravity and density. On Earth, miscible liquids effectively combine into one relatively homogenous (or equally distributed) solution (Pojman et al., 2007). There is no real interface when liquid is perfectly miscible. Surface tension forces in this study are neglected.

The governing equations consist of conservation of mass, momentum and species equations. The conservation of mass and momentum equations are solved to identify the flow fields of the liquids. Species transport by pressure-driven flows occurs as a result of convection and diffusion, and can be described by the combined species convection-diffusion equation. In symbolic notation, the steady state equations can be expressed as

$$\nabla \cdot \vec{U} = 0 \tag{1}$$

$$\rho \vec{U} \cdot \nabla \vec{U} = -\nabla P + \mu \nabla^2 \vec{U} \tag{2}$$

$$\rho \vec{U} \cdot \nabla \phi = D \nabla^2 \phi \tag{3}$$

where $\vec{U}$ is the fluid velocity vector, $\rho$ is the fluid density, $P$ is the pressure, $\mu$ is the fluid dynamic viscosity, $\phi$ is the mass concentration and $D$ is the diffusivity. Eq. (3) must be solved together with Eqs. (1) and (2) in order to achieve computational coupling between the velocity field solution and the concentration distribution.

The computational fluid dynamics package, CFD-ACE+$^{TM}$, which uses a finite volume approach, is utilized to solve the three-dimensional flow fields and mixing of two fluids. A nonlinear steady-state algorithm is used for hydrodynamic calculations, and a linear steady-state algorithm is applied to solve the diffusion-convection equation. Three-dimensional structured grids are used, and the SIMPLEC method is employed for pressure–velocity coupling (Van Doormaal and Raithby, 1984). The spatial discretizations for the convection terms are performed using a second-order upwind scheme with limiter (Barth and Jespersen, 1989) and the spatial discretizations for the diffusion-like terms are then presented applying a second-order central difference scheme. The simulation is implemented for a steady state. A fixed-velocity condition is set at the mixer inlet; the boundary condition at the outlet is a fixed pressure. The concentration of species is normalized to 1 and 0 for the inlet on the right and left sides, respectively. The fluid properties are set as the physical and thermodynamic properties of water at 300 K. The algebraic multigrid (AMG) solver is utilized for pressure corrections (Wienands and Joppich, 2005), and the conjugate gradient squared (CGS) and preconditioning (Pre) solvers are used for velocity and species corrections during an iteration (Sonneveld, 1989). The inertial relaxation for velocities is set to 0.1, and the linear relaxation for pressure is set to 0.5. The solution is considered converged when the relative errors of all transported variables are $<10^{-4}$ between successive sweeps.

This study considers some different flow system configurations. The general configuration consists of some slanted ridges cut onto the top and bottom floors (c.f. Fig. 1(A)). It is composed of two layers. Some ridges are cut on the top layer, and some are etched on the bottom layer. The ridges etched onto the two floors have tangential surfaces. The tangential surface of the two ridges is at the center of the channel. The 45° angle characterizes the orientation of ridges with respect to the channel. Fig. 1(B) shows a top view of the crosswise structural patterns; the proposed micromixer is named as a crosswise ridge micromixer (CRM). The grid systems in the computation domain are chosen to ensure orthogonality, smoothness and low aspect ratios to prevent numerical divergence (Fig. 1(C)). Poor grid systems can enhance numerical diffusion effects. In Eulerian simulations, time and space are divided into discrete grids, and the continuous differential equations of motion are deconstructed into discrete equations. These discrete equations are generally more diffusive than the original differential equations; thus, the behavior of the simulated system differs from that of the intended physical system. If liquid fluids flow diagonally through the simulated grid, then the numerical effect takes the form of an extra high diffusion rate. In the proposed grid systems, meshing is generally aligned in the flow direction in the computational domain. The models do not include the input Y-junction, but rather start directly at the microchannel entrance. To minimize the effects of the meshing on mixing, mesh density is increased continuously until it has minimal effects on the mixing index at the outlet cross section. Grid size sensitivity was analyzed at the very beginning of the numerical simulations and shown in Table 1. The middle case has been chosen for further investigation, since the mixing indices at the three different locations are almost the same. These grids have been chosen to ensure that numerical results are grid-independent.

The uniformity of mixing at sampled sections is assessed by determining the mixing index $\varphi$ of the solute concentration,

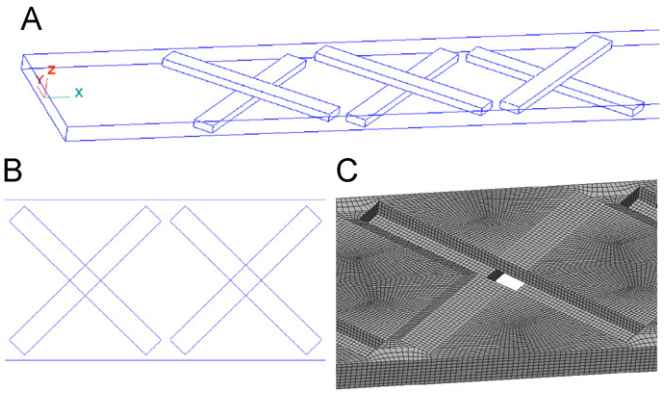


**Fig. 1.** (A) Schematic diagram of the physical features, (B) the channel layout and (C) grid system in the computational domain. The microchannel is 750 μm wide and 90 μm deep.

**Table 1**
Grid sensitivity analysis.

| Number of nodes | Mixing index | | |
|---|---|---|---|
| | $x=0.065$ cm | $x=0.951$ cm | $x=1.842$ cm |
| 724,425 | 11.09% | 36.66% | 54.39% |
| 824,040 | 10.33% | 36.09% | 53.71% |
| 908,600 | 10.23% | 36.04% | 53.68% |

which is defined as

$$\varphi = 1 - \frac{\int_A |I - I_{ave}|\, dA}{\int_{A_0} |I_0 - I_{ave}|\, dA} \tag{4}$$

where $I$ is the concentration value (between 0 and 1) on the sampled section $A$, $I_o$ is the concentration value at the inlet plane $A_0$ and $I_{ave}$ is the averaged value of the concentration over the sampled section. The mixing index $\varphi$ range is from 0 for no mixing to 1 for complete mixing.

## 3. Fabrication process and flow visualization

For experimental characterization of mixing performance of passive micromixers, two different microchannels are fabricated—a microchannel with only crosswise grooves, and a microchannel with slanted ridges on the top and bottom floors of channels. The flow device is fabricated using a replica molding method. Fig. 2 schematically shows the microfabrication process. Initially, a silicon wafer is cleaned and dehydrated on a hotplate (Fig. 2(A)). A thin film is fabricated by spin coating negative photoresist (SU-8) onto a silicon wafer. The resist is then soft baked on a level hotplate (Fig. 2(B)). The channel pattern is fabricated by photolithography, using a chrome photo mask (Fig. 2(C)). After development, the master is washed and baked to fix the photoresist. A wafer with patterned SU-8 is then obtained (Fig. 2(D)). Once the mold is complete, the wafer is rinsed in deionized (DI) water and dried with nitrogen. After pouring the polydimethylsiloxane (PDMS) prepolymer mixture onto the wafer with the patterned SU-8, micro-structures are fabricated using a PDMS molding process with an SU-8 mold (Fig. 2(E)). The PDMS prepolymer mixture is degassed with a mechanical vacuum pump to remove air bubbles. The PDMS is then cured in an oven and the PDMS replicas are peeled off from the master (Fig. 2(F)). The microchannels are designed by forming molds of the upper and lower plate structure via conventional planar lithography. The inlet and outlet holes are then drilled (Fig. 2(G)). Methanol is used as a surfactant to prevent two oxygen-plasma-treated PDMS replicas from being irreversibly bonded when aligned improperly. After $O_2$ plasma treatment and bonding, the designed microchannels are fabricated. A series of crosswise grooves are etched into the bottom floor of a channel, and a series of slanted ridges are etched onto the two floors of a channel (Fig. 2(H)). Fig. 3 shows the scanning electron micrographs (SEM) of the microchannel for one typical micromixer in this study. Some slanted ridges are fabricated near the input Y-junction on one layer of the channel (Fig. 3(A)), and the slanted ridges switch directions inside the channel (Fig. 3(B)). The microchannels are put together by bonding the two same layers. The width, thickness and length of the microchannels are 750 μm, 90 μm and 4 cm, respectively, for all three microchannels. The ridges are 45 μm deep and 890 μm long, and are shown in Fig. 3(A).

For the mixing experiment in pressure-driven flows, two different fluids are injected into the microchannels using a syringe pump (Programmable Syringe Pump, KD Scientific, USA) at preset constant flow rates. The experimental setup for testing the performance of the fabricated micromixers is described as follows. One syringe is loaded with DI water and the other is

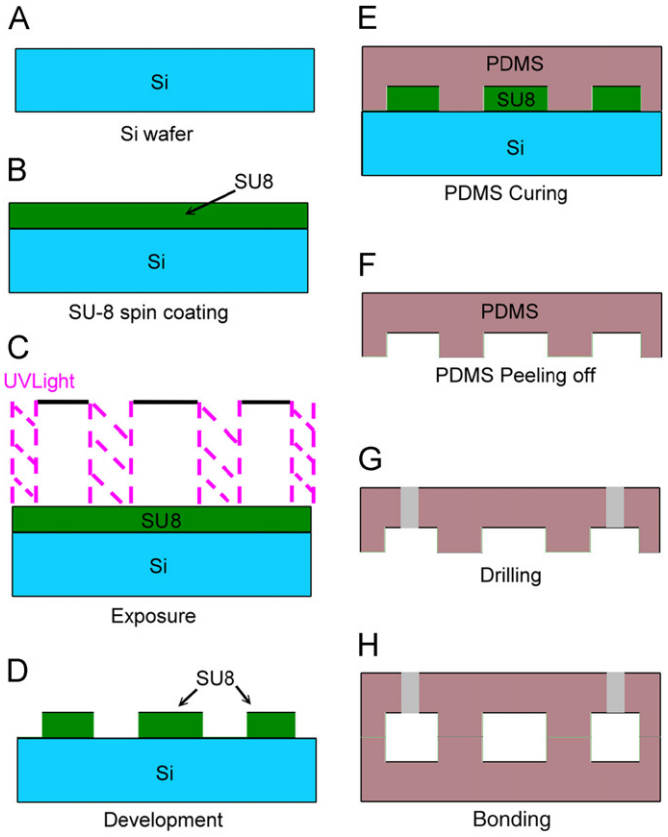


**Fig. 2.** Schematic diagram of the microfabrication process of SU-8 molds and the PDMS micromixers.

loaded with black Quink Ink (Parker, USA). The working fluids first enter the inlet channels, flow through the micromixer, and finally exit through a outlet channel. Several experiments were performed with various flow rates for different micromixers to investigate the effects of operational and geometrical parameters on the mixing performance. Once the steady state is attained, the color changes along the downchannel direction are captured by a microscope and high-speed camera (X-Stream$^{TM}$ XS-4, IDT, USA) at a magnification of 40 × with a graphic grabber system (VCD-Gear TV Plus). To verify the simulation results, a confocal microscope (Leica TCS SP2, Leica Corporation, Germany) is utilized to monitor the mixing behaviors at the cross-sections of the mixing channel. One syringe is filled with fluorescent solution (99% DI water and 1% rhodamine B, Fluka, Germany), while the other is filled with DI water only. The images of the fluorescent solution are excited at 543 nm with a He–Ne green laser and the signal of fluorescent emission can be detected in red (585 to 615 nm). The fluorescence is monitored with a confocal microscope equipped with an air objective (10 × /0.4, ∞/0.17/A). The XY cross-section is scanned with a resolution of 1024 × 1024, and the YZ cross-section is scanned with a resolution of 1024 × 240 (total distance along the $z$-axis is 120 μm with an interval of 1.5 μm). Images are analyzed using image processing software (ImageJ, Version 1.24o). Intensity linescans of the channel cross section at different locations are utilized to determine the amount of mixing.

This study normalizes the color intensities of pictures taken in experiments with each micromixer; i.e., Eq. (5) is used to normalize color intensity of each pixel.

$$I_n = \frac{I - I_{\min}}{I_{\max} - I_{\min}} \tag{5}$$

where $I_{\min}$ is the minimum intensity of a pixel measured from the mixer when DI water flows into the two inlets, $I_{\max}$ is the

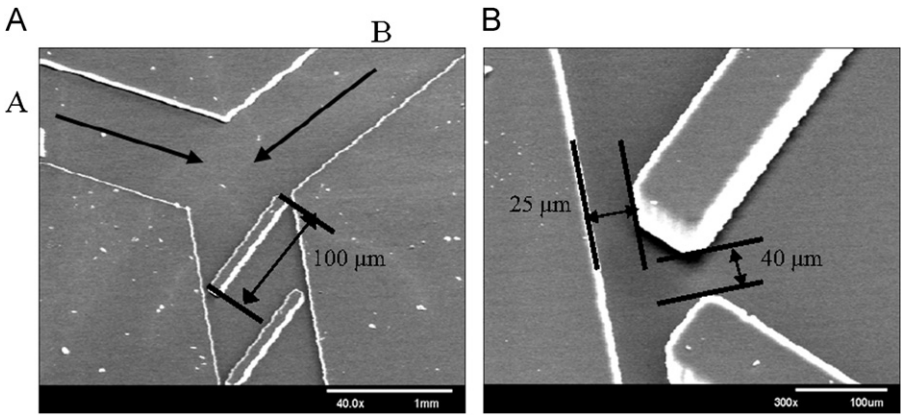


**Fig. 3.** The SEM images of the fabricated microchannel made of PDMS; the magnified image shows the slanted ridges. Two fluids are introduced from channels A and B. The length of the ridges is 100 μm. The gaps between a ridge and channel wall and between ridges are 25 and 40 μm, respectively.

maximum intensity of a pixel measured from the mixer when the fluorescent or black ink solution flows into the two inlets, $I_i$ is the color intensity of a pixel, and $I_n$ is the normalized color intensity of a pixel. The uniformity of the mixing at sampled sections is then evaluated by deriving the mixing index $\varphi$ of the solute concentration, which is the same as that derived by Eq. (4), except that $I$ is replaced by $I_n$. The mixing index ranges from 0 for no mixing to 1 for complete mixing. The micromixers are designed for investigating the effects of various parameters, such as Reynolds number, on mixing characteristics associated with the geometric effect.

## 4. Micromixer design

In this section, the design concept of the crosswise ridge micromixer is introduced. From the preliminary studies on the slanted grooved micromixer (SGM), a rotational motion of the fluids is generated. A repeating unit of the crosswise ridge micromixer (CRM) has a simple two-layer structure consisting of crosswise slanted ridges cut onto the top and bottom floors. The crosswise slanted ridges in the channel create helical flows rotating either clockwise or counterclockwise depending on its orientation, as shown in Fig. 4. Several cross-sectional locations of the structure are expressed with (a), (b), (c), (d), (e), (f), (g) and (h). The first ridge on the top floor slants from left to right, and the ridge on the bottom floor slants from right to left. These ridges create two counterclockwise helical flows side by side within the channel near the location (a). Then two helixes flow toward the central region of the channel. Because the ridges are stacked between locations (b) and (c), no fluids can flow through the central region and the two helixes merge into a single large one. The size of the helical flow decreases (between locations (b) and the blue line shown in Fig. 4), and then increases (between the blue line and locations (c) shown in Fig. 4). After leaving this region, the helical flow splits into two and the helixes approach the wall separately. The next ridges slant in the opposite direction. These ridges create two clockwise helical flows side by side near the location (d). Similar flow characteristics can be observed along the downchannel. A significant amount of split and recombination (SAR) helical flows exist due to fluids flowing through the slanted ridges embedded on the two floors of the channels. The ability to sequentially combine these flow regimes creates much contact surface between two fluids and rapid mixing in the channel.

In order to perform a comprehensive analysis of the mass transfer mechanism in CRM, the cross-sectional concentration distributions are utilized to demonstrate the mixing characteristics along the downstream channel. Besides, in an effort to understand the two-fluid mixing inside the mixer, the velocity vector planes are utilized to demonstrate the rotation of the fluid flows. Fig. 5 shows the bas-relief patterns for the mixer with slanted ridges on its two floors, and several cross-sectional locations of the second structure from the inlets at 1.5, 1.65, 1.85 and 2 mm are also noted with (a), (b), (c) and (d). The cross-sectional velocity vectors change along the downchannel from the outlet at an input flow rate of 100 μl/min (Fig. 5), which corresponds to an inlet flow velocity of 0.05 m/s and Reynolds number of 10. Reynolds number ($Re$) is the ratio of inertia to viscous forces. The void bottom areas in the images represent the solid section of the micromixer. The flow field has two components along the channel. One is the downchannel flow component (dots in Fig. 5). The other one is the transversely rotational flow component. The slanted ridges are on the top and bottom channel floors, and two leading and trailing edges are in the cross-sectional area. The leading edge of the ridge functions as a sink and the trailing edge of the ridge functions as a source. Due to this combination of a source and sink, rotational flows occur in the channel. Vortices are centered on the ridges, and these vortices follow the ridges across the channel. These two components, the downchannel flow component and transversely rotational flow component, result in an overall helical flow inside the microchannel and two counterclockwise flow patterns occur. One counterclockwise flow moves from the left side to the right side, and the other flow moves from the right to left simultaneously. The flow feature of the two helical flows is the main mass transport mechanism of the crosswise patterned mixer. Thus, the helical flows generate superior mixing. Fig. 5 also shows the simulated mixing results at four cross-sectional areas along the channel. The transversely rotational flow pushes the fluid across the channel central line. An enlarged interfacial surface area is increased considerably. These images (Fig. 5) show the stretching of the two fluids, indicating that mixing can be improved. The fluorescence in confocal images is classified into two regions, namely bright and dark regions. The confocal images differ a little from the simulation. Some of the bright regions in confocal images overlap the solid sections of the micromixer; this is because of the light scattering effects occurring at the crosswise ridges. However, it can be observed that the bright region stretches to the dark region, because of the transversely rotational flow.

This work examines a microchannel with a flat floor and a microchannel with the crosswise grooves on the bottom floors to confirm the performance of the CRM. This study analyzes three different configurations of a microfluidic system via numerical simulations and experimental measurements. The top views of

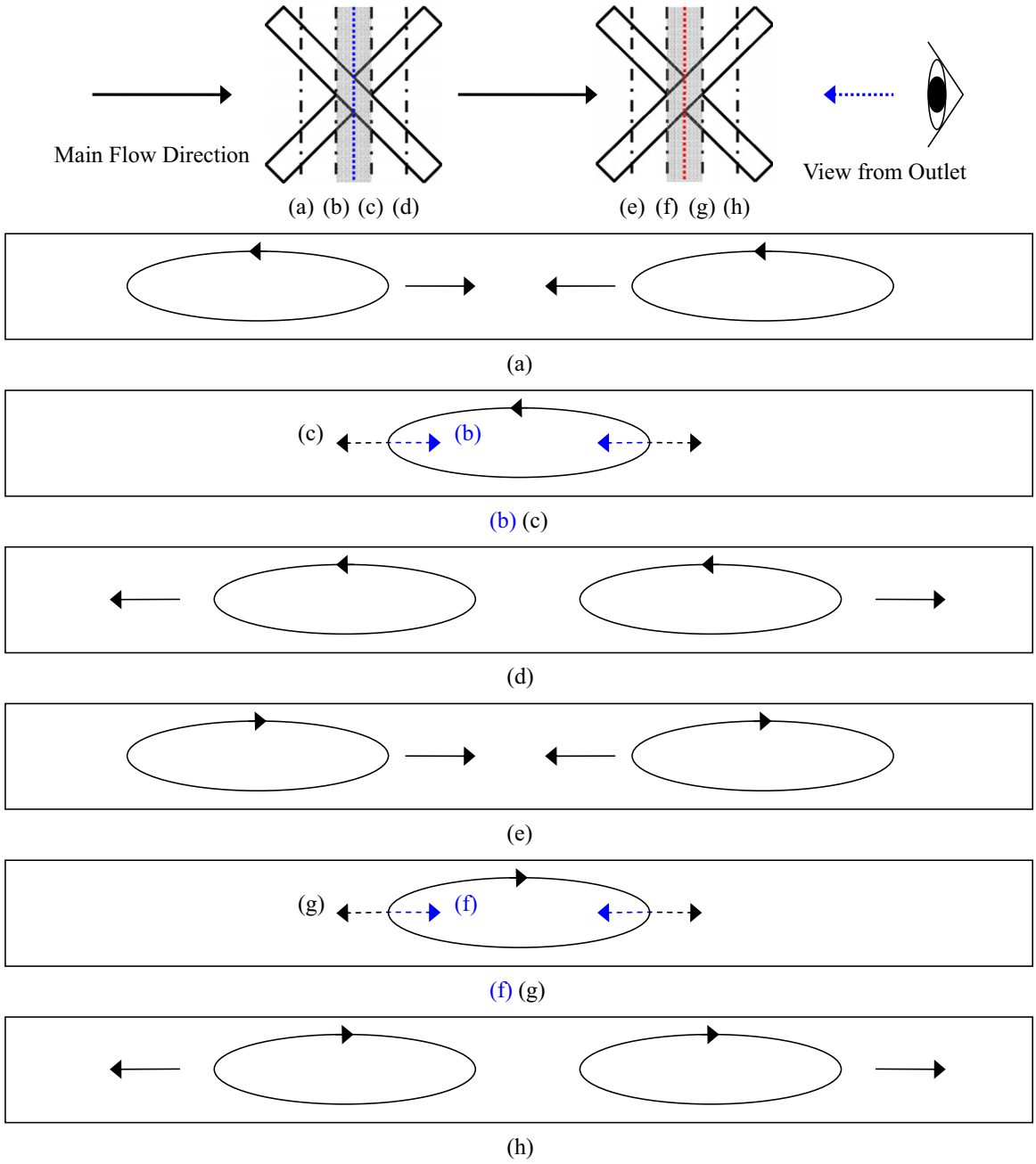


**Fig. 4.** The lateral flow patterns along the downchannel generated by the crosswise slant ridges. (For interpretation of the references to color in this figure, the reader is referred to the web version of this article.)

the images along the downchannel direction were commonly used to qualitatively characterize the mixing performance of the micromixer. In our work, the top view of the color changes along the downchannel direction are captured by a microscope and high-speed camera with a graphic grabber system. The microchannels are 750 μm wide, 90 μm deep and 4 cm long. The experimental mixing results for each micromixer are taken at five representative positions, 0, 1, 2, 3 and 4 cm beyond the Y-junction in the downchannel direction. The above parameters' values are utilized unless specified otherwise. Fig. 6 presents experimental results of each micromixer at five representative positions along the downchannel direction, when DI water and ink–water solutions are injected through each inlet at an *Re* of 10. For the Y-type mixer shown in Fig. 6(A), two parallel streams meet at the exact center of the channel and, thus, the interface is clearly observed in the front section of the channel. This result shows that the flow field in this channel is essentially a laminar flow to the channel end. The mixing of two fluids is only through molecular diffusion across the interface of the two liquids. A sufficiently long channel length is needed to complete the mixing. The crosswise grooves on the bottom floors (Fig. 6(B)) only generate a slight improvement in mixing between the two fluids in the microchannel, and the interface of the two fluids is not evident. The two fluids mix only around the channel central line from the Y-junction to the outlet; that the mixing process can be achieved very rapidly is not obvious. Since the crosswise grooves on the bottom floors are symmetrical with the microchannel central line, the distortions in the interface of two fluids are caused by the crosswise microstructures and/or small differences in velocities at the two inlets (this phenomenon is discussed

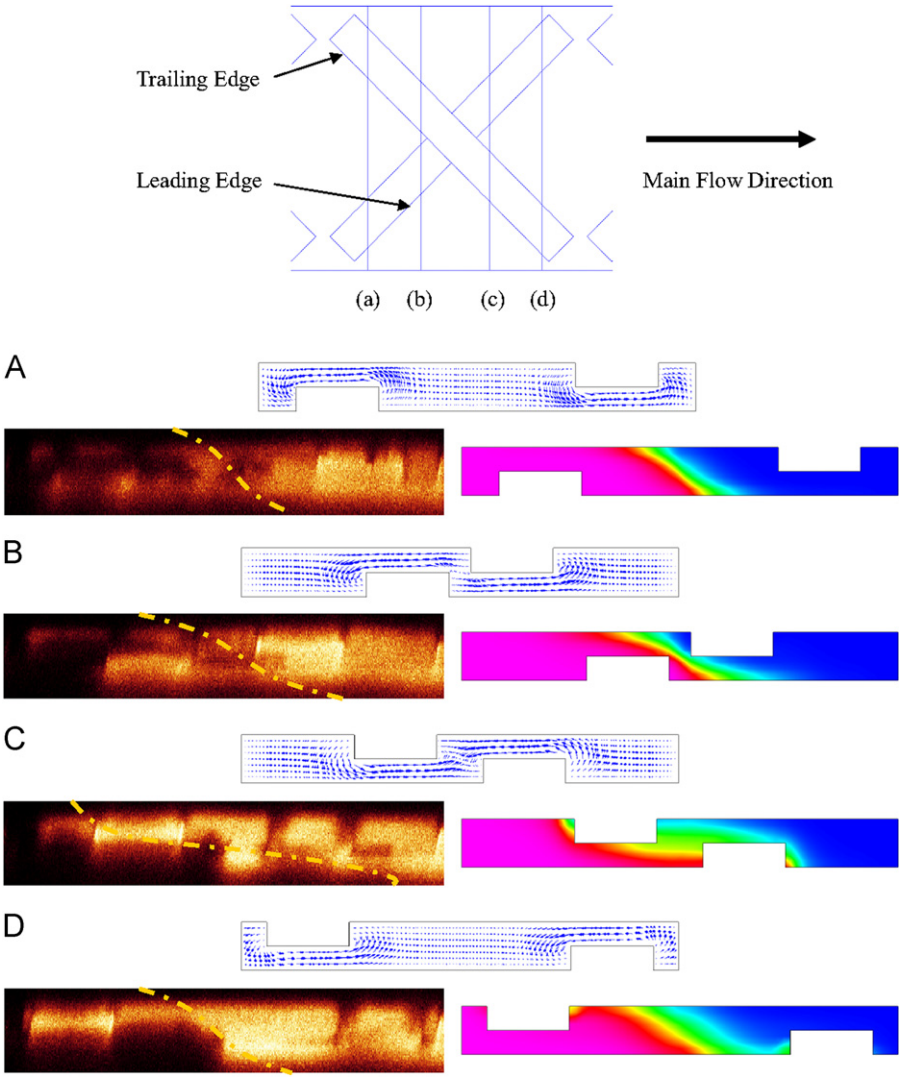


**Fig. 5.** The locations of cross-sections from (a) to (d). The vector planes and mixing characteristics at four cross-sectional areas along the downchannel. And the cross-sectional images of experimental mixing patterns observed with a confocal microscope.

later). The interface of the two fluids remains clear until they reach the outlet, demonstrating that mixing is limited by pure diffusion and is very poor. In Fig. 6(C), the ink–water solution is spread across the channel and broken up into several separate streams. The number of ridges per cycle is 4. The first two ridges at the top floor slant from left to right, and those at the bottom floor slant from right to left. The next two ridges slant in the opposite directions. At the end of the channel, the mixed fluids are well dispersed across the channel. Notably, due to the increases of the interfaces of the two fluids, mixing is improved by placing slanted ridges on the top and bottom floors.

Simulation results are presented and compared with experimental data at two specific positions. Fig. 7 lists the numerical mixing characteristics of the above three micromixers from Fig. 6(A) to (C) compared with experimental results. These experimental results are taken at two specific positions, 0 and 1 cm beyond the Y-junction along the downchannel direction, and the flow conditions are the same as those in cases from Fig. 6(A) to (C). Among the numerical results shown in Fig. 7, the fluid with blue color is representative of the black Quink Ink and the fluid with red color represents the DI water. In the Y-type mixer, two fluids meet at the centerline along the downchannel (Fig. 7(A)). Mixing performance is almost negligible; this numerical result is the same as the experimental result. The crosswise grooves in the crosswise groove mixer are symmetrical with the central line in Fig. 7(B). The two fluids reach the front edges of the grooves at the same positions, enter the grooves, flow beneath the main stream from the side edges to the central line, meet at the central line and flow back to the side edge. Because the structures are symmetrical, the liquid flowing through the grooves cannot enter the main stream section of the other fluid. Thus, the two fluids are mixed only via a molecular diffusion process. Notably, contact surface of the two fluids cannot be increased. The inlet velocities of the blue and red liquids are set at 0.051 and 0.05 m/s, respectively. The interface of the two fluids is not coincident with the channel central line, because the inertial forces of the two fluids differ. The two fluids flow to the front edges of the crosswise grooves and enter the grooves. The fluid with the fastest inlet velocity has a large inertial force and can push the other fluid away from the channel's central line; thus, the interface of two fluids is no longer coincident with the symmetrical axis. The mixing performance is slightly improved as a result. This study examines the mixing characteristics of the cross-wise ridge mixer with slanted ridges on its two floors, which is shown in Fig. 7(C). The two fluids reach the front edges of the ridges at the same positions, flow along the ridges from the side edges to the central line, meet at the central line, flow across the ridges, reach

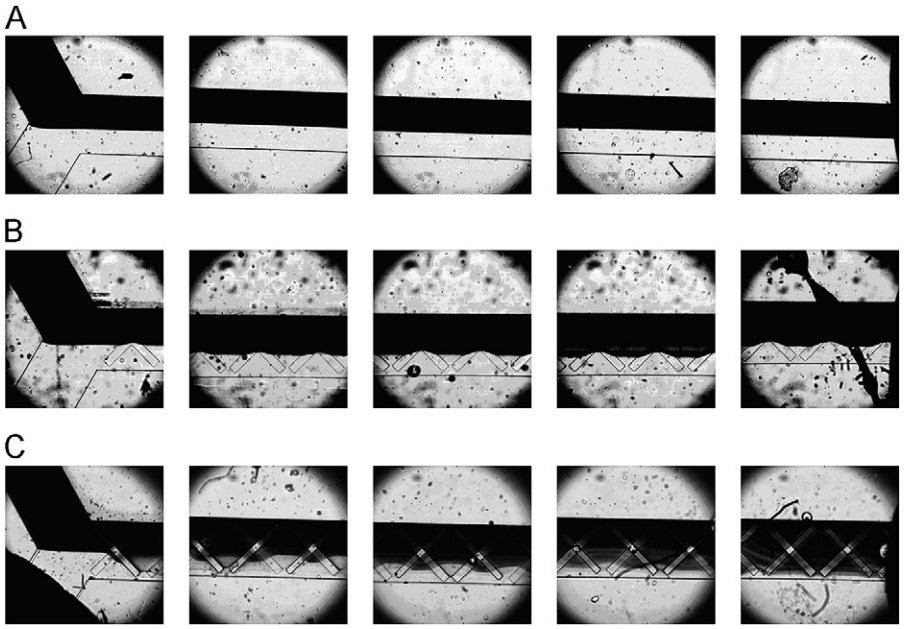


**Fig. 6.** Top viewed photographs of the experimental mixing results shown from left to right are taken at five representative positions, 0, 1, 2, 3 and 4 cm beyond the Y-junction in the downchannel direction. (A) The Y-type mixer, (B) the crosswise groove mixer with crosswise grooves on the bottom floors and (C) the crosswise ridge mixer with slanted ridges on the top and bottom floors when Reynolds number is 10.

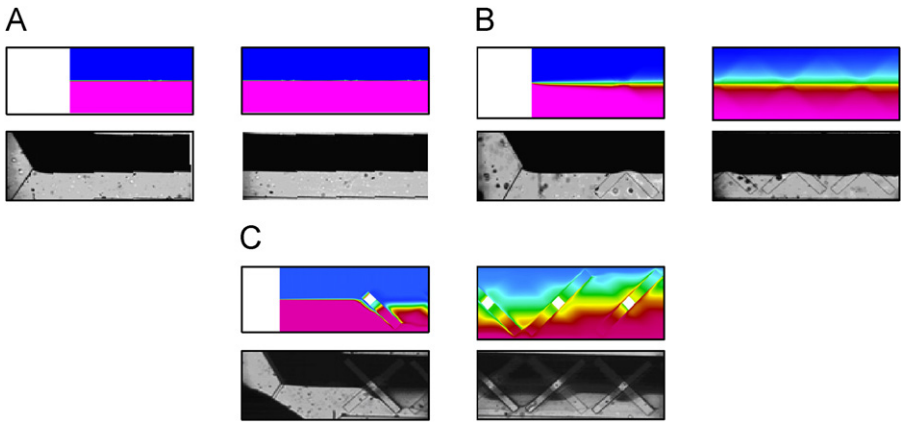


**Fig. 7.** Numerical mixing results for the (A) Y-type mixer, (B) crosswise groove mixer with crosswise grooves on the bottom floors and (C) crosswise ridge mixer with slanted ridges on the top and bottom floors. These numerical results are compared with experimental results at representative positions of 0 and 1 cm beyond the Y-junction along the downchannel direction. (For interpretation of the references to color in this figure legend, the reader is referred to the web version of this article.)

the side edge and roll back to the central line. The contact areas of two fluids are increased drastically and the diffusion distance is decreased significantly. Mixing is greatly enhanced.

The results are compared with the previous work of Fu et al. (2006): staggered oriented ridges static micromixers (SOR). In every mixing segment of their design, the microstructure consisted of microchannels and two pairs of ridges. Two ridges are located in the top layer, while the other two are located in the bottom layer. Their results show that the interface between the two streams is distorted as it moves downstream, and a significant amount of stirring accompanies an *Re* of 57.93. This stirring is a continuous deformation of the interface and redistribution of the stream. The top views of the mixing performance of the CRM at different representative positions along the downchannel direction are demonstrated in Fig. 8. The input flow rate in our crosswise ridge micromixer is equal to 500 μl/min, which corresponds to an *Re* of 50. Good mixing at the channel end has been achieved. The interface between streams is indistinct as they move downstream, shown in Fig. 8(A). In addition, the fluids flow along the ridges, reach the side edge and roll back to the central line. The interfaces of two fluids are increased drastically. The geometric design of the proposed SOR is modified and scaled to be of similar size to that of our mixer. In their design, the value of $w$ is 750 μm, $h$ is 90 μm, $q$ is 1480 μm, $s1$ and $s2$ are 375 μm, and $\theta$ is 45°. Numerical results are compared with our mixer by utilizing the mixing index at every two mixing segments. In Fig. 8(B), mixing index is plotted against the segments of the micromixers. It is revealed that the mixing index moves up relative to an increase in the number of mixer segments for each mixer considered. The ridges on the top and bottom layer in Fu's group's work have tangent planes. The tangent position of two staggered ridges is not at the center of the channel. And the ridges are not stretched to the side walls. The slanted ridges from one side of the channel to the other are etched onto the top and bottom floors of a channel in CRM. The interface is stretched much more for our mixer than that of an SOR, so the mixing index of our mixer is always higher than that of an SOR.

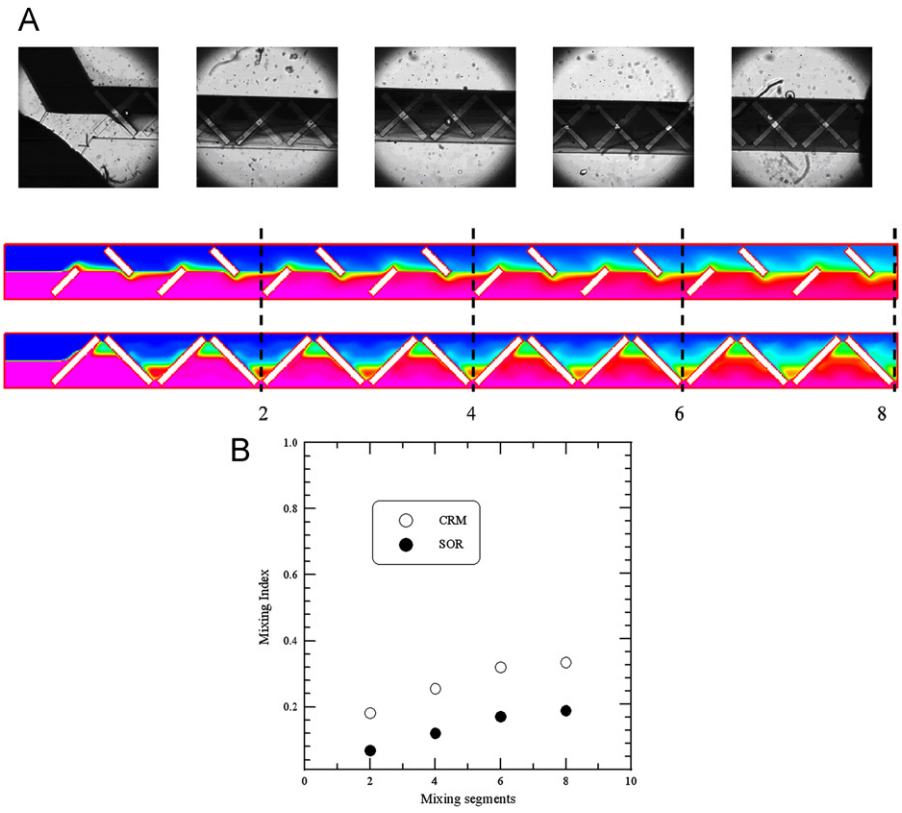


**Fig. 8.** Comparison results with the previous study (Fu et al., 2006): (A) photographs of mixing at $Re=50$ in CRM and (B) the mixing index vs. number of mixing segments.

## 5. Results and discussion

The effects of various Reynolds numbers on flow fields and mixing characteristics inside the microfluidic system are examined first. The effects of the number of crosswise patterns on mixing performance of microchannels are then investigated. The experimental results for the crosswise ridge mixer (CRM) with ridges on the top and bottom floors are studied, and the effects of various inlet velocities on mixing characteristics are analyzed. An *Re* of 0.05, 0.1, 1, 10 and 50 are considered; these numbers correspond to inlet flow velocities of 0.00025, 0.0005, 0.005, 0.05 and 0.25 m/s, respectively. In Fig. 9, the mixing index at five specific locations of 0, 1, 2, 3 and 4 cm are calculated at various *Re*. The dashed line represents a mixing index equal to 0.9, and the mixing length is the channel length required for achieving the mixing index of 0.9. Linear regression is utilized to predict the mixing index at different locations for each *Re*. The linear model can be expressed as $\varphi = ax+b$, where $\varphi$ is the mixing index and $x$ is the location distance from the inlet. From each linear equation, the predicted mixing length can be obtained by setting the mixing index equal to 0.9. The resulting mixing lengths are 4.86, 6.16, 6.41, 4.91 and 3.65 cm at an *Re* of 0.05, 0.1, 1, 10 and 50, respectively. Because the inertial force of the fluids was so small that it is negligible at $Re=0.05$, mixing is dominated by pure molecular diffusion. The time of contact between two fluids is sufficiently long enough to generate significant mixing with a mixing length of $<5$ cm. As the *Re* rises gradually, the viscous force of fluids is still dominant, and the effects of various *Re* on mixing are not distinct. However, the mixing length for $0.1<Re<1$ is longer than that at an *Re* equal to 0.05. For $Re>1$, the mixing length decreases with increasing *Re*; the increased inertial force enlarges the contact area between two fluids. When the *Re* is 50, good mixing at the channel end has been achieved. The interface between streams is indistinct as they move downstream. By the naked eye, one can see that mixing in the channel increases as the *Re* increases (Fig. 8(A)).

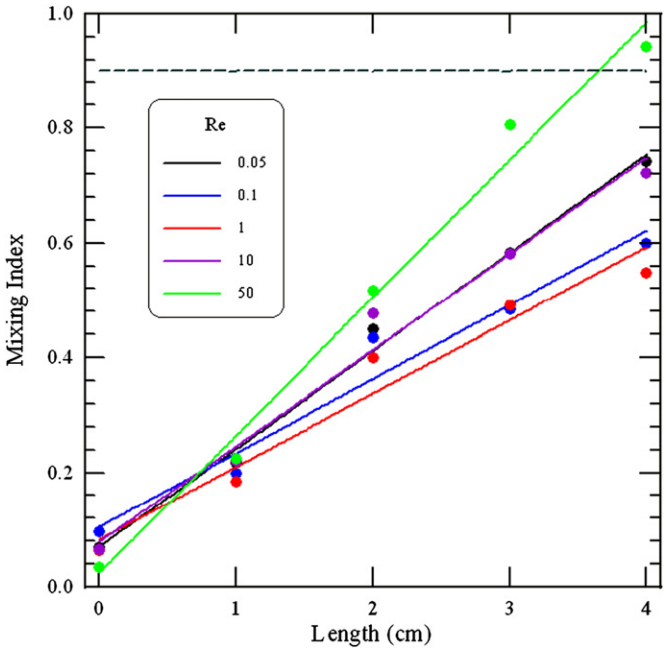


**Fig. 9.** Experimental mixing indices for various Reynolds numbers at different locations. The dashed line represents that the mixing index is equal to 0.9, and the mixing length is the channel length required for achieving the mixing index of 0.9.

The experimental mixing capability of the CRM with ridges on the top and bottom floors at several *Re* is quantified (Fig. 10) by comparison with numerical results. Each normalized intensity is plotted at the abscissa corresponding to different *Re*. At low *Re*,

$0.05 < Re < 1$, viscous forces in the fluid are larger than inertial forces; thus, inertia can be neglected. Fluid velocity in a channel cross section is essentially two-dimensional, and the flow creeps through the ridged channels. Therefore, no lateral transportation exists and the interface is not distorted; only the positions of the fluids change. Mixing within the stated range of the *Re* is dominated by pure molecular diffusion. Mixing improves at an *Re* of 0.05 due to the corresponding increase in residence time. Residence time is generally a useful concept that states how fast something moves through a system. In a microfluidic system, residence time is the average time fluids spend within a particular microchannel. The velocity of the fluid is slow when the *Re* is small; thus, residence time increases. Therefore, two different fluids have increased time to mix via pure diffusion. The mixing index then decreases as the *Re* increases within the range 0.05–1. When the *Re* are 1–50, both viscous and inertial forces are important. Consequently, the flow around a ridge will be three-dimensional, with secondary flows generated in the channel cross section in addition to the bulk flow along the channel axis. These secondary flows, combined with the axial flow, distort and stretch material interfaces. Thus, the size of the interfacial area across which diffusion occurs at increases markedly, leading to rapid mixing. Thus, when the *Re* is 50, mixing performance is improved. Fig. 10 shows simulation results at the location of 1.5 cm, which are compared with experimental results. Results show that the normalized average intensity changes at various *Re*. Because of the numerical diffusion in the computational domain, the mixing index at the specific location by numerical simulation is larger than that by experimental measurement, and not identical. However, the trends of the experimental results and numerical data are very similar.

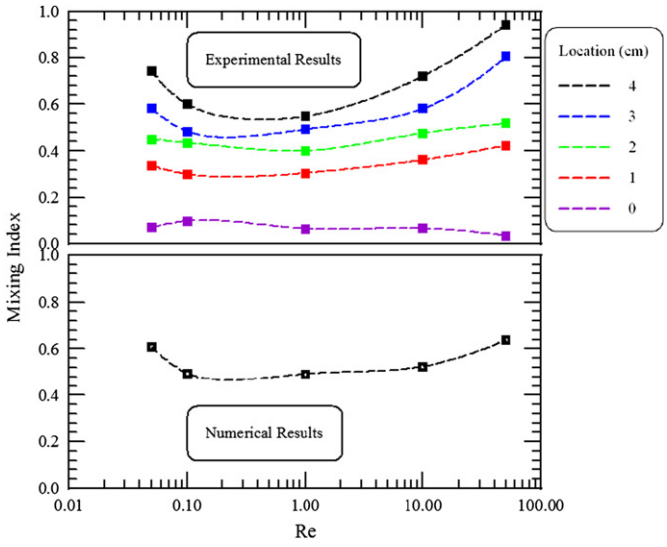


**Fig. 10.** Experimental and numerical mixing indices for various Reynolds numbers at different locations.

The mixer has several mixing segments. A mixing segment is composed of two consecutive regions of ridges, i.e., two half-cycles. The direction in which the ridges slant changes relative to the channel centerline from one region to every other half cycle.

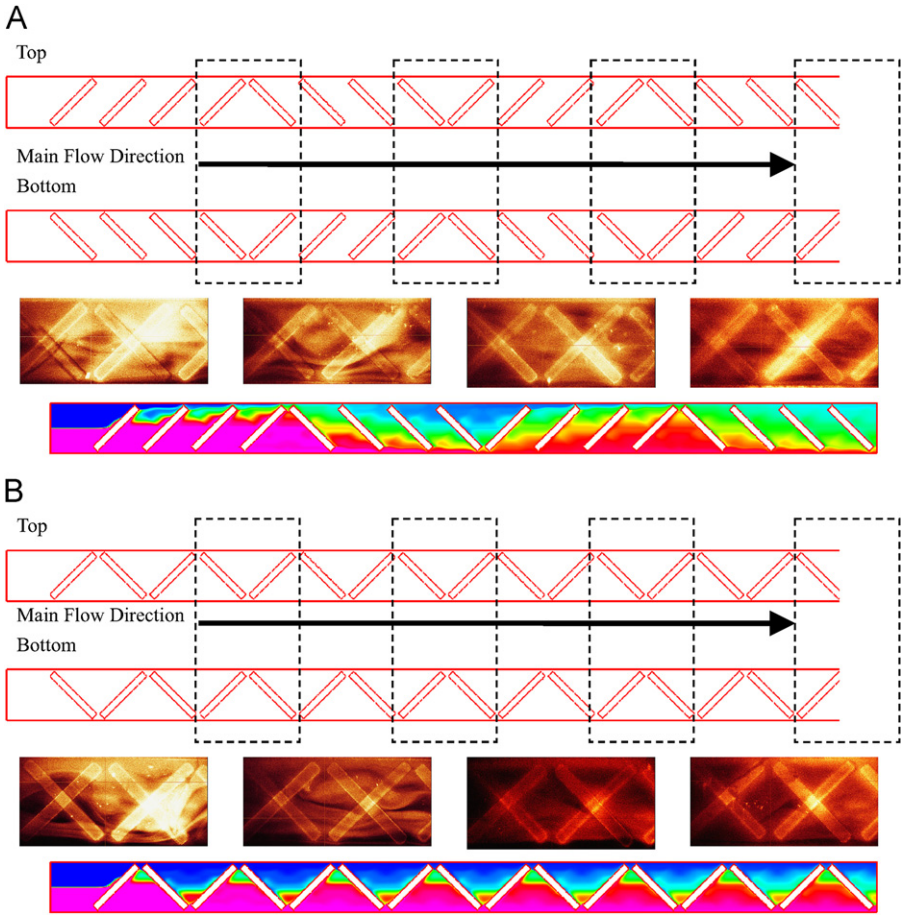


**Fig. 11.** Schematic representation of the channel layout and the direction of the flow. Mixing characteristics for various numbers of ridges in the channels per cycle: (A) 8 and (B) 2 ridges are placed on the floors in one cycle.

The schematic representation of the channel layout and the direction of the flow are shown in Fig. 11. This study presents the effects of the number of ridges per cycle on mixing quality. Two and eight ridges are placed on the floors in one cycle (Fig. 11(A) and (B)) at an *Re* of 50. The orientations of the ridges are the same in each half cycle. The confocal images are taken at four representative positions marked by the rectangular box (Fig. 11). Two liquid fluids flow along the ridges from the side edges to the central line, flow across the ridges and reach the side edge. When the number of ridges per cycle is 2, the interface of the two fluids is stretched after they pass through the previous ridge. The area of the interface is then decreased after passing through the next ridge with changing direction. The fluids flow across the channel central line and then soon flow back to the initial regions, when the number of the ridges in one cycle is 2. The change in ridge slant direction redirects the fluids toward the channel centerline. Thus, the contact area along the downchannel is reduced and mixing is poor. As the number of ridges in one cycle increases to 8, the stretching effect of the two fluids increases and a high mixing index is attained. Numerical results are compared with the experimental results, and they correlate well with each other.

The effects of various numbers of ridges per cycle on the mixing quality are then shown. In Fig. 12(A), the orientation of all patterns is in the same direction, and the concentration distribution from the top view is shown. Of about 16, 8, 4 and 2 ridges are placed on the floors in one cycle and are represented in Fig. 12(B), (C), (D) and (E). The mixing indexes are 0.736, 0.708, 0.642, 0.556 and 0.393 at an *Re* equal to 50. The more ridges per half cycle, the more pronounced effect of fluid spreading is and higher mixing indexes are achieved. The mixing performances of the crosswise ridge mixer with different numbers of ridges on two floors at several *Re* are demonstrated in Fig. 12(F). The mixing index is 0.736 for ridges placed with the same orientation. It indicates that the stretching of two fluids cannot be more distinct when the number of ridges per cycle is equal to eight or above. Thus, the mixing performance achieves optimum value in case, where the number of ridges per cycle is equal to 8.

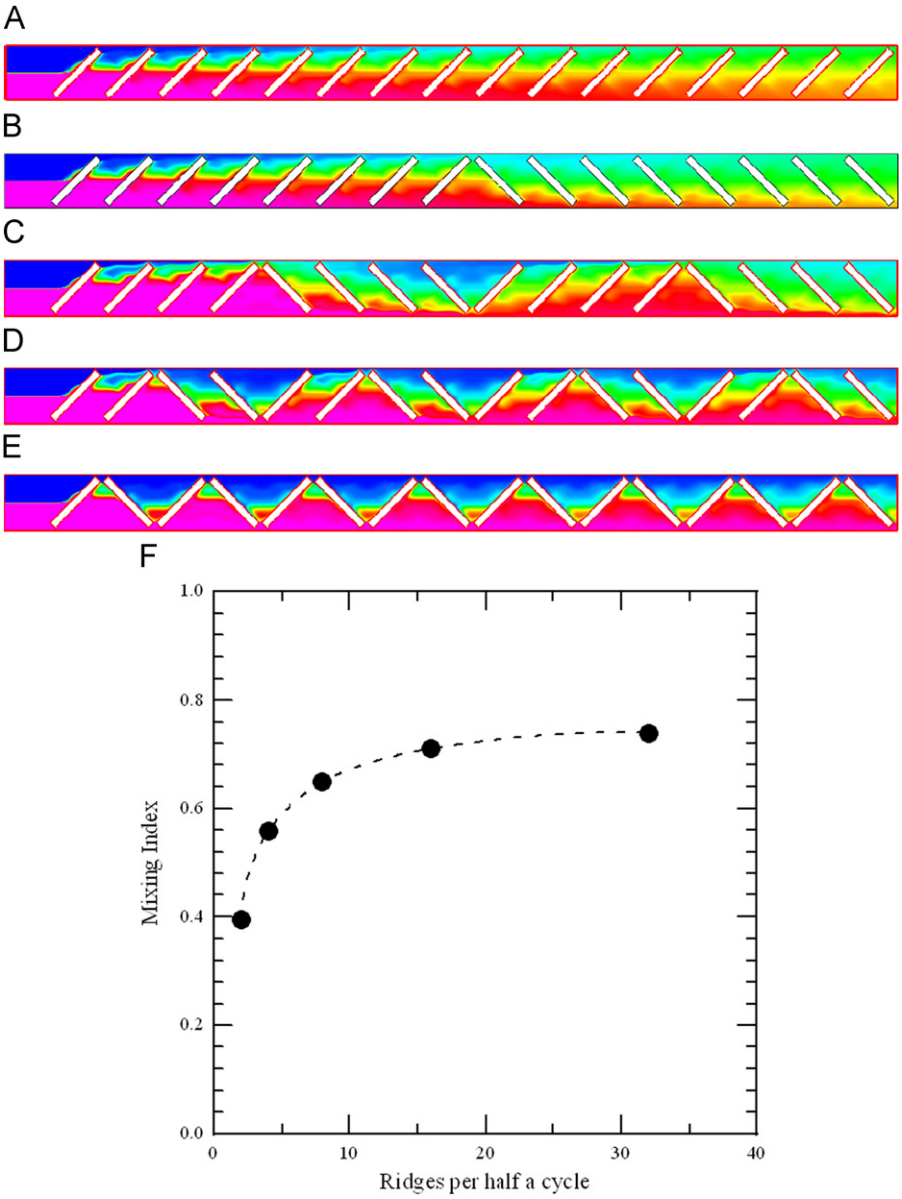


**Fig. 12.** The mixing characteristics for various numbers of the ridges per cycle. (A) The orientation of all patterns is in the same direction. (B), (C), (D) and (E) are 16, 8, 4 and 2 ridges are placed on the floors in one cycle, respectively. (F) The mixing performances of the CRM with different numbers of ridges on two floors.

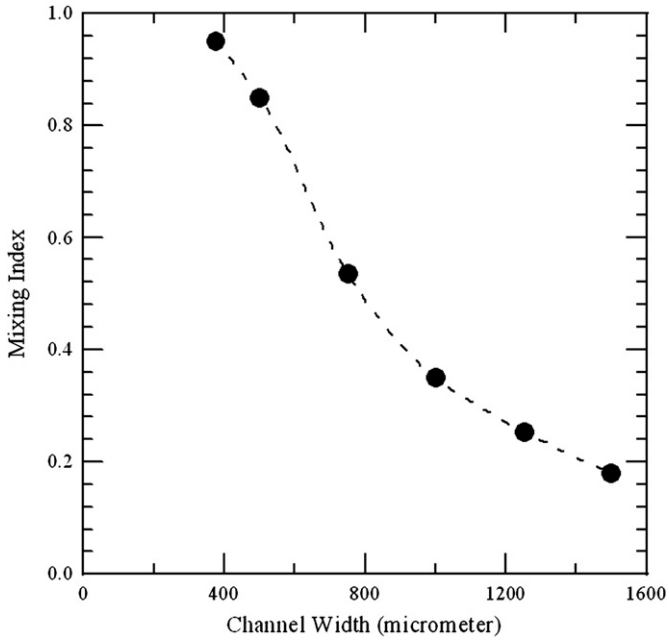


**Fig. 13.** The mixing performances of the CRM with different channel widths.

The effects of the geometric parameters on mixing are critical in the design of the micromixers. Several studies have examined the relationship between the ridge design and the mixing performance. Earlier experimental tests proved that the 45° angle characterizing the orientation of the ridges with respect to the channel is the most appropriate (Liu et al., 2005). Wang et al. (2003a) investigated influences of the ridge height on mixing. When the size of ridges becomes larger, the lateral velocity increases, and so does mixing efficiency. In previous works, the effects of the channel height on the mixing length at a constant flow rate (Gobby et al., 2001) and at a constant cross-sectional area (Wang et al., 2002) were examined. Results showed that a minimum exists at an aspect ratio of channel height to channel width, when the flow rate is constant. In our work, the width, thickness and length of the microchannels are 750 μm, 90 μm and 4 cm, respectively, for all microchannels. The height of the ridges is 45 μm and is shown in Fig. 3(A). The ratio of the ridge height to the channel thickness is 0.5. The effects on mixing of ratios of the ridge height to the channel thickness, which are 1/2, 1/3, 1/4 and 0, are examined and not shown in this article. Results show that the largest mixing index is obtained when the ratio of the ridge height to the channel thickness is equal to 0.5. A significant amount of split and recombination (SAR) helical flows are also produced in this case. As the ratio of the ridge height to the channel thickness decreases, the mixing index is decreased due to pure diffusion. For two fluids flowing parallel in a channel, the diffusion occurs at the interface of the two fluids. This interfacial area is distorted and increased, resulting in rapid mixing. Finally we show influences of various channel widths on the mixing. Four ridges are placed on the floors in one cycle at an *Re* of 10. The mixing indexes at five specific channel widths of 1500, 1000, 750, 500 and 375 μm are calculated with a constant value of channel height (i.e., 90 μm) in Fig. 13. The inlet velocity increases as the channel width decreases at a constant *Re*. The layout of ridges gives different resistances to the flow, and the fluids follow the path with lower flow resistance. Then, part of the fluid is distorted and redirected to the area without ridges. The fluid velocity near the ridges is increased further to keep the mass conservation. Thus, interface between the two streams is distorted as it moves downstream, and a significant amount of stirring accompanies this distortion. It is found in Fig. 13 that when keeping a fixed *Re* the mixing index decreases by increasing the channel width.

## 6. Conclusions

This study elucidated the mixing characteristics of two fluids in a crosswise ridge micromixer (CRM) via numerical and experimental studies associated with microchannels with various inlet velocities. The mixer is fabricated in PDMS using standard MEMS technology. A three-dimensional computational model is proposed for mixing two fluids. Analytical results are presented in terms of concentration distributions and velocity vector planes. Fluid flows are simulated to investigate the mixing indexes of the fluids and/or velocity vectors at cross-sectional regions. For microchannels with crosswise ridges on the top and bottom floors, the downchannel and transversely rotational flows result in helical flows along the downchannel. Mixing performance is significantly influenced by the split and recombination (SAR) helical flows and depends on Reynolds number. Experimental results demonstrate that the micromixer with slanted ridges embedded on the top and bottom floors of channels has excellent mixing efficiency, and the mixing index increases when Reynolds number is increased to 50. The confocal images at the cross-sections along the channel with ridges on both the channel top and bottom are first investigated in our study. Some of the bright regions in confocal images overlap the solid sections of the micromixer, because of the light scattering effects occurring at the crosswise ridges. Numerical results are also compared with experimental measurements and show similar trends for distributions of concentrations and the mixing indexes of the two fluids. Finally the effects of various numbers of crosswise ridges in one cycle of the channels are also examined. Geometric changes significantly affect the mixing of liquids in the microchannel. The orientations of ridges have a considerable effect on the direction of fluids. Thus the mixing performance achieves an optimum value in case where the number of ridges per cycle is equal to 8. The major goals of this paper are to investigate the physical insights of the flow characteristics and the mixing performances in the crosswise ridge micromixers. The readers are referred to good literatures for a full discussion about the effects of the ridge designs on mixing. Our future work is to optimize the crosswise ridge design by systematically integrating a CFD package with an optimization methodology based on the use of design of experiments. From the transport point of view, the three-dimensional steady or unsteady flow leads to much faster dispersion than the two-dimensional unsteady flow does. This should lead to better mixing (Cartwright et al., 1996). We should be reporting in future work a time-dependent three-dimensional computation to perform a comprehensive analysis of the mass transfer mechanism in crosswise ridge micromixer.

## Acknowledgments

The authors would like to thank the National Science Council of the Republic of China, Taiwan, for financially supporting this research under Contract no. NSC96-2221-E-020-021-. And we are grateful to the National Nano Device Laboratories for MEMS processes. Daryl Switak is appreciated for his editorial assistance.

## References

Ansari, M.A., Kim, K.Y., 2007. Shape optimization of a micromixer with staggered herringbone groove. Chemical Engineering Science 62 (23), 6687–6695.

Aubin, J., Fletcher, D.F., Bertrand, J., Xuereb, C., 2003. Characterization of the mixing quality in micromixers. Chemical Engineering & Technology 26 (12), 1262–1270.

Aubin, J., Fletcher, D.F., Xuereb, C., 2005. Design of micromixers using CFD modeling. Chemical Engineering Science 60 (8-9), 2503–2516.
Barth, T.J., Jespersen, D.C., 1989. The design and application of upwind schemes on unstructured meshes. 27th Aerospace Sciences Meeting and Exhibit, Reno, Nevada, USA, AIAA-89-0366.
Bhagat, A.A.S., Peterson, E.T.K., Papautsky, I., 2007. A passive planar micromixer with obstructions for mixing at low Reynolds numbers. Journal of Micromechanics and Microengineering 17 (5), 1017–1024.
Branebjerg, J., Gravesen, P., Krog, J.P., Nielsen, C.R., 1996. Fast mixing by lamination. In: Proceedings of the Ninth IEEE International Workshop Micro Electromechanical System, MEMS '96, San Diego, CA, USA, 441–446.
Camesasca, M., Manas-Zloczower, I., Kaufman, M., 2005. Entropic characterization of mixing in microchannels. Journal of Micromechanics and Microengineering 15 (11), 2038–2044.
Cartwright, J.H.E., Feingold, M., Piro, O., 1996. Chaotic advection in three-dimensional unsteady incompressible laminar flow. Journal of Fluid Mechanics 316, 259–284.
Cortes-Quiroz, C.A., Zangeneh, M., Goto, A., 2009. On multi-objective optimization of geometry of staggered herringbone micromixer. Microfluidics and Nanofluidics 7 (1), 29–43.
Cussler, E.L., 1984. Diffusion Mass Transfer in Fluid Systems. Cambridge University Press, New York.
Fu, X., Liu, S., Ruan, X., Yang, H., 2006. Research on staggered oriented ridges static micromixers. Sensors and Actuators, B: Chemical 114 (2), 618–624.
Gobby, D., Angeli, P., Gavriilidis, A., 2001. Mixing characteristics of T-type microfluidic mixers. Journal of Micromechanics and Microengineering 11 (2), 126–132.
Hasssell, D.G., Zimmerman, W.B., 2006. Investigation of the convective motion through a staggered herringbone micromixer at low Reynolds number flow. Chemical Engineering Science 61 (9), 2977–2985.
Howell Jr., P.B., Mott, D.R., Fertig, S., Kaplan, C.R., Golden, J.P., Oran, E.S., Ligler, F.S., 2005. A microfluidic mixer with grooves placed on the top and bottom of the channel. Lab on a Chip 5 (5), 524–530.
Incropera, F.P., DeWitt, D.P., 1990. Fundamentals of Heat and Mass Transfer third ed. John Wiley & Sons, Inc., New York.
Johnson, T.J., Ross, D., Locascio, L.E., 2002. Rapid microfluidic mixing. Analytical Chemistry 74 (1), 45–51.
Jones, S.W., Thomas, O.M., Aref, H., 1989. Chaotic advection by laminar flow in a twisted pipe. Journal of Fluid Mechanics 209, 335–357.
Kang, T.G., Kwon, T.H., 2004. Colored particle tracking method for mixing analysis of chaotic micromixers. Journal of Micromechanics and Microengineering 14 (7), 891–899.
Kang, T.G., Singh, M.K., Kwon, T.H., Anderson, P.D., 2008. Chaotic mixing using periodic and aperiodic sequences of mixing protocols in a micromixer. Microfluidics and Nanofluidics 4 (6), 589–599.
Kim, D.S., Lee, S.W., Kwon, T.H., Lee, S.S., 2004. A barrier embedded chaotic micromixer. Journal of Micromechanics and Microengineering 14 (6), 798–805.
Li, C., Chen, T., 2005. Simulation and optimization of chaotic micromixer using lattice Boltzmann method. Sensors and Actuators, B: Chemical 106 (2), 871–877.
Lim, D., Kamotani, Y., Cho, B., Mazumder, J., Takayama, S., 2003. Fabrication of microfluidic mixers and artificial vasculatures using a high-brightness diode-pumped Nd:YAG laser direct write method. Lab on a Chip 3 (4), 318–323.
Liu, R.H., Stremler, M.A., Sharp, K.V., Olsen, M.G., Santiago, J.G., Adrian, R.J., Aref, H., Beebe, D.J., 2000. Passive mixing in a three-dimensional serpentine microchannel. Journal of Microelectromechanical Systems 9 (2), 190–197.
Liu, S., Fu, X., Yang, H., 2005. Research of a 3D static micro-mixer with staggered oriented ridges. Chinese Journal of Mechanical Engineering 41 (4), 132–136.
Miyake, R., Lammerink, T.S.J., Elwenspoek, M., Fluitman, J.H.J., 1993. Micro mixer with fast diffusion. In: Proceedings of the Sixth IEEE International Workshop Micro Electromechanical System, MEMS '93, Fort Lauderdale, FL, USA, 248–253.
Mobius, H., Ehrfeld, W., Hessel, V., Richter, T., 1995. Sensor controlled processes in chemical microreactors. In: Proceedings of the Eighth International Conference on Solid-State Sensors and Actuators, Transducers '95, Stockholm, Sweden, 775–778.
Nguyen, N.T., Wu, Z., 2005. Micromixers—a review. Journal of Micromechanics and Microengineering 15 (2), R1–R16.
Oddy, M.H., Santiago, J.G., Mikkelsen, J.C., 2001. Electrokinetic instability micromixing. Analytical Chemistry 73 (24), 5822–5832.
Ottino, J.M., Wiggins, S., 2004. Introduction: mixing in microfluidics. Philosophical Transactions, Series A, Mathematical, Physical, and Engineering Sciences 362 (1818), 923–935.
Pojman, J.A., Bessonov, N., Volpert, V., 2007. Miscible fluids in microgravity (MFMG): a zero-upmass investigation on the international space station. Microgravity Science and Technology 19 (1), 33–41.
Schonfeld, F., Hardt, S., 2004. Simulation of helical flows in microchannels. AIChE Journal 50 (4), 771–778.
Sonneveld, P., 1989. CGS, a fast Lanczos-type solver for nonsymmetric linear systems. SIAM Journal on Scientific and Statistical Computing 10 (1), 36–52.
Stroock, A.D., Dertinger, S.K.W., Ajdari, A., Mezic, I., Stone, H.A., Whitesides, G.M., 2002. Chaotic mixer for microchannels. Science 295 (5555), 647–651.
Van Doormaal, J.P., Raithby, G.D., 1984. Enhancements of the simple method for predicting incompressible fluid flows. Numerical Heat Transfer 7, 147–163.
Voldman, J., Gray, M.L., Schmidt, M.A., 2000. An integrated liquid mixer/valve. Journal of Microelectromechanical Systems 9 (3), 295–302.
Wang, H., Iovenitti, P., Harvey, E., Masood, S., 2002. Optimizing layout of obstacles for enhanced mixing in microchannel. Smart Materials and Structures 11 (5), 662–667.
Wang, H., Iovenitti, P., Harvey, E., Masood, S., 2003a. Passive mixing in microchannels by applying geometric variations. Proceedings of SPIE 4982, 282–289.
Wang, H., Iovenitti, P., Harvey, E., Masood, S., 2003b. Numerical investigation of mixing in microchannels with patterned grooves. Journal of Micromechanics and Microengineering 13 (6), 801–808.
Wienands, R., Joppich, W., 2005. Practical Fourier Analysis for Multigrid Methods. Chapman and Hall/CRC, Virginia Beach.
Yang, J.T., Huang, K.J., Lin, Y.C., 2005. Geometric effects on fluid mixing in passive grooved micromixers. Lab on a Chip 5 (10), 1140–1147.